JOC Article
pubs.acs.org/joc

Lipophilic β-Cyclodextrin Cyclic−Nitrone Conjugate: Synthesis and Spin Trapping Studies

Yongbin Han,[†,⊥] Yangping Liu,[‡] Antal Rockenbauer,[§] Jay L. Zweier,[‡] Grégory Durand,[¶] and Frederick A. Villamena*[,†,‡]

[†]*Department of Pharmacology and* [‡]*Center for Biomedical EPR Spectroscopy and Imaging, The Davis Heart and Lung Research Institute, College of Medicine, The Ohio State University, Columbus, Ohio 43210,* [§]*Chemical Research Center, Institute of Structural Chemistry, H-1025 Budapest, Pusztaszeri 59, Hungary, and* [¶]*Laboratoire de Chimie BioOrganique et des Systèmes Moléculaires Vectoriels, Faculté des Sciences, Université d'Avignon et des Pays de Vaucluse, 33 Rue Louis Pasteur, 84000 Avignon, France.* [⊥]*Current address: Technical Institute of Physics and Chemistry, Chinese Academy of Sciences, Beijing 100190, China*

frederick.villamena@osumc.edu

Received April 24, 2009

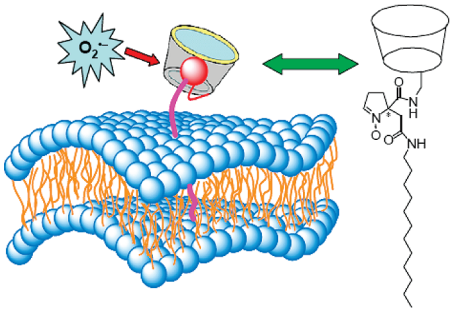

Nitrone spin traps are commonly employed as probes for the identification of transient radicals in chemical and biological systems using electron paramagnetic resonance (EPR) spectroscopy. Nitrones have also found applications as therapeutic agent in the treatment of radical-mediated diseases. Therefore, a spin trap that incorporates high reactivity to superoxide radical anion ($O_2^{\bullet-}$), more persistent superoxide adduct, enhanced bioavailability, and selective targeting in one molecular design is desirable. In this work, the synthesis of a nitrone spin trap, **4**, that is tethered via amide bonds to a β-cyclodextrin (β-CD) and a dodecyl chain was achieved with the expectation that the β-cyclodextrin would lead to increased reactivity to $O_2^{\bullet-}$ and persistent $O_2^{\bullet-}$ adduct while the lipophilic chain would impart membrane targeting property. The two constitutional racemic isomers, **4a** and **4b**, were separated using preparative HPLC, and structural analysis and self-aggregation properties were carried out using NMR, induced circular dichroism, dynamic light scattering, transmission electron microscopy, and computational approach. EPR spin trapping of $O_2^{\bullet-}$ by **4a** and **4b** was only successful in DMSO and not in an aqueous system, due most likely to the amphiphilic character of **4** that can favor conformations (or aggregation) hindering radical addition to nitrone. Kinetics of formation and decay of the **4a**-O_2H adduct in polar aprotic solvents show faster reactivity to $O_2^{\bullet-}$ and more persistent $O_2^{\bullet-}$ adduct compared to nitrones not conjugated to β-CD. Computational analysis of **4a** and **4b** as well as **4a**-OOH and **4b**-OOH adducts were carried out, and results show that isomerism, both constitutional and stereochemical, affects the orientations of aminoxyl-NO and/or hydroperoxyl groups relative to the β-CD annulus for optimal H-bond interaction and stability.

Introduction

Spin trapping using nitrone spin traps and electron paramagnetic resonance (EPR) spectroscopy is commonly employed for the identification and detection of free radicals.[1] The use of spin trapping has been gaining popularity in the investigation of reactive intermediates in the areas of fuel cell

*To whom correspondence should be addressed. Phone: +1 614-292-8215. Fax: +1 614-688-0999. E-mail: frederick.villamena@osumc.edu.

(1) Villamena, F. A.; Zweier, J. L. *Antioxid. Redox Signaling* **2004**, *6*, 619–629.

DOI: 10.1021/jo900856x Published on Web 06/16/2009

research,[2] nanotechnology,[3] catalysis,[4] environmental remediation,[5] and photodynamic therapy.[6] Moreover, the ability of nitrones to trap radicals makes them suitable as antioxidants in the treatment of reactive oxygen species-mediated pathophysiological disorders such as neurodegenerative disease,[7] acute stroke,[8,9] cancer,[9] and ischemia-reperfusion injury.[10] However, the "antioxidant" property of nitrone spin traps is not clear but goes beyond direct radical scavenging by suppressing pro-apoptotic signal transduction and gene induction processes that can lead to oxidative stress.[11]

The slow reactivity of nitrones to $O_2^{\bullet-}$ and the short half-life of their corresponding spin adducts as well as their passive diffusion through cell membranes limit their application in biological systems as an $O_2^{\bullet-}$ probe.[12] We previously reported[13,14] that cyclic nitrone derivatization at the C-5 position with an amide moiety such as in the case of 5-carbamoyl-5-methyl-1-pyrroline-*N*-oxide (AMPO) increases electrophilicity of the nitronyl carbon and therefore gives an enhanced reactivity to $O_2^{\bullet-}$ compared to 5,5-dimethyl-1-pyrroline-*N*-oxide (DMPO),[15] 5-ethoxycarbonyl-5-methyl-1-pyrroline-*N*-oxide (EMPO),[16] and 5-diethoxyphosphoryl-5-methyl-1-pyrroline-*N*-oxide (DEPMPO) (Figure 1).[17] Moreover, this increased reactivity of amide-derivatized nitrones to $O_2^{\bullet-}$ is facilitated by intramolecular H-bonding interaction between the amide-H and $O_2^{\bullet-}$ at the transition state.[13] We therefore postulated that an amide linker group can provide opportunities for conjugation and still maintains enhanced reactivity to $O_2^{\bullet-}$. Computational and experimental studies showed that intramolecular H-bond interaction contributes to $O_2^{\bullet-}$ adduct stability.[18] We also showed[19] that the presence of flexible H-bond acceptors contributes to $O_2^{\bullet-}$ adduct stability compared to rigid H-bond acceptors such as in the case of the spirolactonyl-nitrone, CPCOMPO (Figure 1).

In the early 1970s, Birrell et al.[20] were the first to observe the EPR spectra of the inclusion complex from γ-cyclodextrin (γ-CD) and the spin-labeled 7-doxylstearic acid showing an anisotropic motion along the *z*-axis. Several inclusion studies then followed,[21] and it was reported[22] that the rate of reduction of some nitroxides by ascorbic acid was significantly decreased in the presence of β-CD, indicating the protective property of β-CD. The synthesis of methylated β-CD,[23] Me_3CD-PBN (Figure 1), showed improved adduct stability for $O_2^{\bullet-}$ with $t_{1/2} \sim 10$ min compared to the PBN-$O_2^{\bullet-}$ adduct alone with a half-life of < 1 min. We demonstrated that β-CD−cyclic nitrone conjugate (β-CDMPO)[24] shows the highest rate for spin trapping of $O_2^{\bullet-}$ ($58\ M^{-1}\ s^{-1}$) and longest half-life for $O_2^{\bullet-}$ adduct (28 min) observed so far compared to the most commonly used spin traps such as DMPO, DEPMPO, and EMPO. These improved spin trapping properties for β-CDMPO were made possible by exploiting the advantage of using amide linker[13] for improved rate of $O_2^{\bullet-}$ trapping and intramolecular H-bond interactions for adduct stability.[18] However, although β-CDMPO may provide controlled intracellular delivery of nitrone by making it less susceptible to bioreduction, its target specificity remains a limitation. The main mechanism for intracellular uptake of β-CD is through receptor-mediated endocytosis, and this has been shown to be followed by release into the cytosol.[25] Therefore, introduction of a target ligand could actively transport the spin trap−β-CD conjugate to its target destination whether it be in the cytosol, cell membrane, or mitochondria. There have been studies made to support the applicability of CDs as a target delivery vehicle. In fact, β-CD was employed as a nonviral vector for the nuclear delivery of nucleic acids via conjugation to polycations.[26]

Indeed, natural cyclodextrins, due to their high external hydrophilicity exhibit limited affinity toward biological membranes. To overcome this limitation, several types of

(2) (a) Bosnjakovic, A.; Kadirov, M. K.; Schlick, S. *Res. Chem. Intermed.* **2007**, *33*, 677–687. (b) Danilczuk, M.; Bosnjakovic, A.; Kadirov, M. K.; Schlick, S. *J. Power Sources* **2007**, *172*, 78–82. (c) Bosnjakovic, A.; Schlick, S. *J. Phys. Chem. B* **2006**, *110*, 10720–10728.
(3) (a) Ionita, P.; Conte, M.; Gilbert, B. C.; Chechik, V. *Org. Biomol. Chem.* **2007**, *5*, 3504–3509. (b) Babu, S.; Velez, A.; Wozniak, K.; Szydlowska, J.; Seal, S. *Chem. Phys. Lett.* **2007**, *442*, 405–408. (c) Kagan, V. E.; et al. *Toxicol. Lett.* **2006**, *165*, 88–100.
(4) Fu, H.; Zhang, L.; Zhang, S.; Zhu, Y.; Zhao, J. *J. Phys. Chem. B* **2006**, *110*, 3061–3065.
(5) (a) Xiao, G.; Wang, X.; Li, D.; Fu, X. *J. Photochem. Photobiol., A* **2008**, *193*, 213–221. (b) Chang, Q.; He, H.; Zhao, J.; Yang, M.; Qu, J. *Environ. Sci. Technol.* **2008**, *42*, 1699–1704. (c) Yu, J. C.; Ho, W.; Yu, J.; Yip, H.; Wong, P. K.; Zhao, J. *Environ. Sci. Technol.* **2005**, *39*, 1175–1179.
(6) (a) Zeng, Z.; Zhou, J.; Zhang, Y.; Qiao, R.; Xia, S.; Chen, J.; Wang, X.; Zhang, B. *J. Phys. Chem. B* **2007**, *111*, 2688–2696. (b) Rajendran, M.; Inbaraj, J. J.; Gandhidasan, R.; Murugesan, R. *J. Photochem. Photobiol., A* **2006**, *182*, 67–74. (c) Mroz, P.; Pawlak, A.; Satti, M.; Lee, H.; Wharton, T.; Gali, H.; Sarna, T.; Hamblin, M. R. *Free Radical Biol. Med.* **2007**, *43*, 711–719.
(7) Thomas, C. E. In *Neuroprotection in CNS Diseases*; Baer, P. R., Beal, M. F., Eds.; Informa Health Care: New York, 1997; pp 183−204.
(8) Floyd, R. A. *Aging Cell* **2006**, *5*, 51–57.
(9) Floyd, R. A.; Kopke, R. D.; Choi, C.-H.; Foster, S. B.; Doblas, S.; Towner, R. A. *Free Radical Biol. Med.* **2008**, *45*, 1361–1374.
(10) (a) Bradamante, S.; Jotti, A.; Paracchini, L.; Monti, E.; Morti, E. *Eur. J. Pharmacol.* **1993**, *234*, 113–116. (b) Maurelli, E.; Culcasi, M.; Delmas-Beauvieux, M. C.; Gallis, J. L.; Miollan, M.; Tron, T.; Pietri, S. *Free Radical Biol. Med.* **1999**, *27*, 34–41. (c) Pietri, S.; Liebgott, T.; Frejaville, C.; Tordo, P.; Culcasi, M. *Eur. J. Biochem.* **1998**, *254*, 256–265. (d) Tosaki, A.; Braquet, P. *Am. Heart J.* **1990**, *120*, 819–830.
(11) (a) Floyd, R. A.; Hensley, K. *Ann. N.Y. Acad. Sci.* **2000**, *899*, 222–237. (b) Floyd, R. A.; Liu, R. J.; Wong, P. K. In *Handbook of Synthetic Antioxidants*; Packer, L., Cadenas, E., Eds.; Marcel Dekker, Inc.: New York, 1997; pp 339−350.
(12) Khan, N.; Wilmot, C. M.; Rosen, G. M.; Demidenko, E.; Sun, J.; Joseph, J.; O'Hara, J.; Kalyanaraman, B.; Swartz, H. M. *Free Radical Biol. Med.* **2003**, *34*, 1473–1481.
(13) Villamena, F. A.; Xia, S.; Merle, J. K.; Lauricella, R.; Tuccio, B.; Hadad, C. M.; Zweier, J. L. *J. Am. Chem. Soc.* **2007**, *129*, 8177–8191.
(14) Villamena, F. A.; Rockenbauer, A.; Gallucci, J.; Velayutham, M.; Hadad, C. M.; Zweier, J. L. *J. Org. Chem.* **2004**, *69*, 7994–8004.
(15) Finkelstein, E.; Rosen, G. M.; Rauckman, E. J. *J. Am. Chem. Soc.* **1980**, *102*, 4994–4999.
(16) Olive, G.; Mercier, A.; Le Moigne, F.; Rockenbauer, A.; Tordo, P. *Free Radical Biol. Med.* **2000**, *28*, 403–408.
(17) Frejaville, C.; Karoui, H.; Tuccio, B.; Le Moigne, F.; Culcasi, M.; Pietri, S.; Lauricella, R.; Tordo, P. *J. Chem. Soc., Chem. Commun.* **1994**, 1793–1794.
(18) (a) Villamena, F. A.; Hadad, C. M.; Zweier, J. L. *J. Am. Chem. Soc.* **2004**, *126*, 1816–1829. (b) Villamena, F. A.; Merle, J. K.; Hadad, C. M.; Zweier, J. L. *J. Phys. Chem. A* **2005**, *109*, 6089–6098.
(19) Han, Y.; Tuccio, B.; Lauricella, R.; Rockenbauer, A.; Zweier, J. L.; Villamena, F. A. *J. Org. Chem.* **2008**, *73*, 2533–2541.
(20) Birrell, B. G.; Griffith, H. O.; French, D. *J. Am. Chem. Soc.* **1973**, *95*, 8171–8172.
(21) (a) Michon, J.; Rassat, A. *J. Am. Chem. Soc.* **1979**, *101*, 995–996. (b) Martinie, J.; Michon, J.; Rassat, A. *J. Am. Chem. Soc.* **1975**, *97*, 1818–1823.
(22) Okazaki, M.; Kuwata, K. *J. Phys. Chem.* **1985**, *89*, 4437–4440.
(23) Bardelang, D.; et al. *Chem.—Eur. J.* **2007**, *13*, 9344–9354.
(24) Han, Y.; Tuccio, B.; Lauricella, R.; Villamena, F. A. *J. Org. Chem.* **2008**, *73*, 7108–7117.
(25) Ravoo, B. J. In *Cyclodextrin Vesicles for Drug Delivery*. *Cyclodextrin: From Basic Research to Market*, 10th International Cyclodextrin Symposium; Ann Arbor, MI, 2000; pp 168−172.
(26) (a) Choi, H. S.; Yamashita, A.; Ooya, T.; Yui, N.; Akita, H.; Kogure, K.; Ito, R.; Harashima, H. *ChemBioChem* **2005**, *6*, 1986–1990. (b) Kulkarni, R. P.; Wu, D. D.; Davis, M. E.; Fraser, S. E. *Proc. Natl. Acad. Sci. U.S.A.* **2005**, *102*, 7523–7528. (c) Kulkarni, R. P.; Mishra, S.; Fraser, S. E.; Davis, M. E. *Bioconjugate Chem.* **2005**, *16*, 986–994.

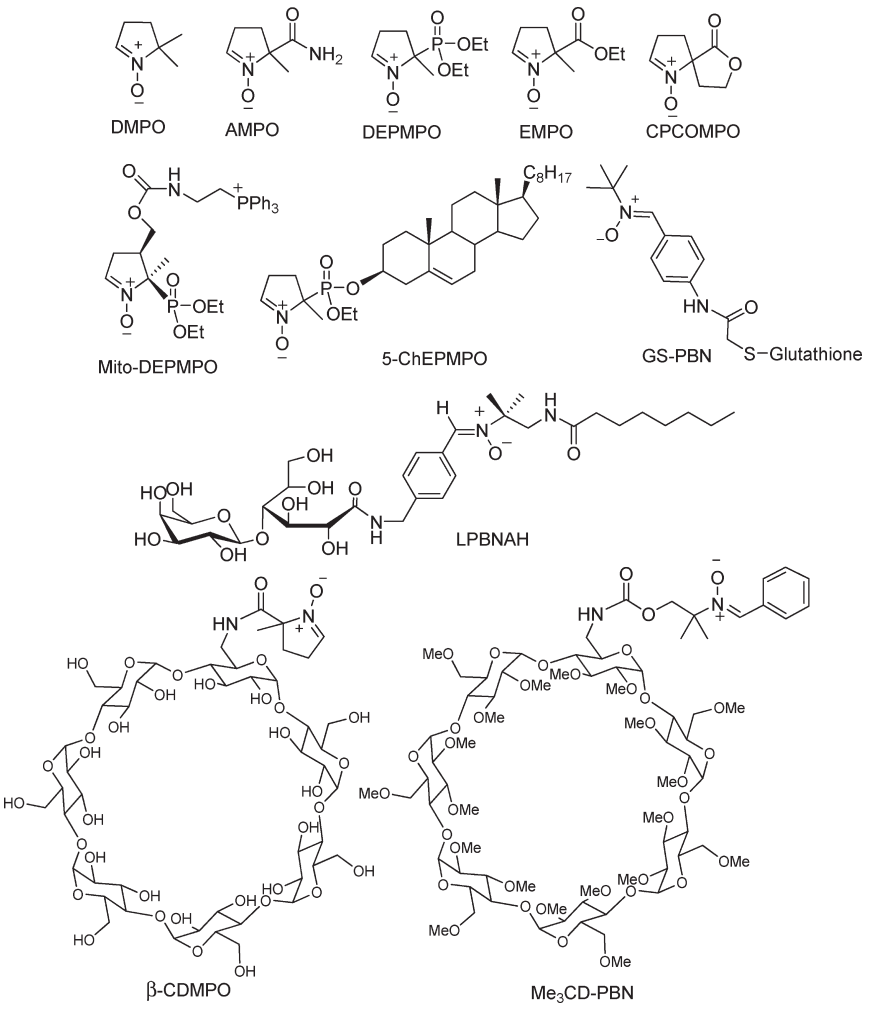

FIGURE 1. Examples of functionalized nitrones.

amphiphilic cyclodextrins have been developed.[27] Among the recently designed amphiphilic cyclodextrins, the monosubstituted cyclodextrins at the C_6 position are promising. Of particular interest are the "lollipops" which result from the grafting of an aliphatic chain on a 6-amino-β-cyclodextrin,[28] their ammonium derivatives,[29] as well as peptidolipidyl derivatives in which an L-leucine spacer arm links the saccharide moiety and the alkyl chain.[30] This amphiphilic structure could perhaps facilitate delivery of the nitrone across the cell membrane and should exhibit higher intracellular (or membrane) accumulation. Indeed, several amphiphilic nitrones have been previously synthesized showing biological activity in in vitro,[31] ex vivo,[32] as well as in vivo models.[33] In the presence of a co-conjugate (i.e., dodecyl group), our expectation is that the dodecyl group could impart membrane affinity and may allow the nitrone to locate very close to the membrane of the cell or organelle. It is well-known that lipophilic antioxidants exhibit membrane affinity as, for instance, vitamin E has been shown to localize within the cellular membranes and lipophilic modification to CDs has been shown to bestow cell-membrane permeation ability.[34]

The idea of bifunctionalizing the nitrone to accommodate target-specific groups has become attractive. For example, a variety of functionalized nitrones have been synthesized such as the LPBNAH,[31] GS-PBN,[35] Mito-DEPMPO,[36] and 5-ChEPMPO[37] (Figure 1). Although these nitrone-conjugated compounds may exhibit a selective targeting of cellular

(27) Duchêne, D.; Ponchel, G.; Wouessidjewe, D. *Adv. Drug Delivery Rev.* **1999**, *36*, 29–40.
(28) Bellanger, N.; Perly, B. *J. Mol. Struct.* **1992**, *273*, 215–226.
(29) Petter, R. C.; Salek, J. S.; Sikorski, C. T.; Kumaravel, G.; Lin, F. T. *J. Am. Chem. Soc.* **1990**, *112*, 3860–3868.
(30) Angelova, A.; Fajolles, C.; Hocquelet, C.; Djedaini-Pilard, F.; Lesieur, S.; Bonnet, V.; Perly, B.; Lebas, G.; Mauclaire, L. *J. Colloid Interface Sci.* **2008**, *322*, 304–314.
(31) (a) Durand, G.; Poeggeler, B.; Boeker, J.; Raynal, S.; Polidori, A.; Pappolla, M. A.; Hardeland, R.; Pucci, B. *J. Med. Chem.* **2007**, *50*, 3976–3979. (b) Durand, G.; Polidori, A.; Ouari, O.; Tordo, P.; Geromel, V.; Rustin, P.; Pucci, B. *J. Med. Chem.* **2003**, *46*, 5230–5237. (c) Durand, G.; Polidori, A.; Salles, J.-P.; Pucci, B. *Bioorg. Med. Chem. Lett.* **2003**, *13*, 859–862.
(32) Tanguy, S.; Durand, G.; Reboul, C.; Polidori, A.; Pucci, B.; Dauzat, M.; Obert, P. *Cardiovasc. Drugs Ther.* **2006**, *20*, 147–149.
(33) (a) Asanuma, T.; et al. *Chem. Biodiversity* **2007**, *4*, 2253–2267. (b) Poeggeler, B.; Durand, G.; Polidori, A.; Pappolla, M. A.; Vega-Naredo, I.; Coto-Montes, A.; Baker, J.; Hardeland, R.; Pucci, B. *J. Neurochem.* **2005**, *95*, 962–973.
(34) Shao, Z.; Li, Y.; Chermak, T.; Mitra, A. K. *Pharm. Res.* **1994**, *11*, 1174–1179.
(35) Liu, Y. P.; Ji, Y. Q.; Song, Y. G.; Liu, K. J.; Liu, B.; Tian, Q.; Liu, Y. *Chem. Commun.* **2005**, *39*, 4943–4945.
(36) Hardy, M.; Chalier, F.; Ouari, O.; Finet, J.-P.; Rockenbauer, A.; Kalyanaraman, B.; Tordo, P. *Chem. Commun.* **2007**, *10*, 1083–1085.
(37) Hardy, M.; Ouari, O.; Charles, L.; Finet, J.-P.; Lacazio, G.; Monnier, V.; Rockenbauer, A.; Tordo, P. *J. Org. Chem.* **2005**, *70*, 10426–10433.

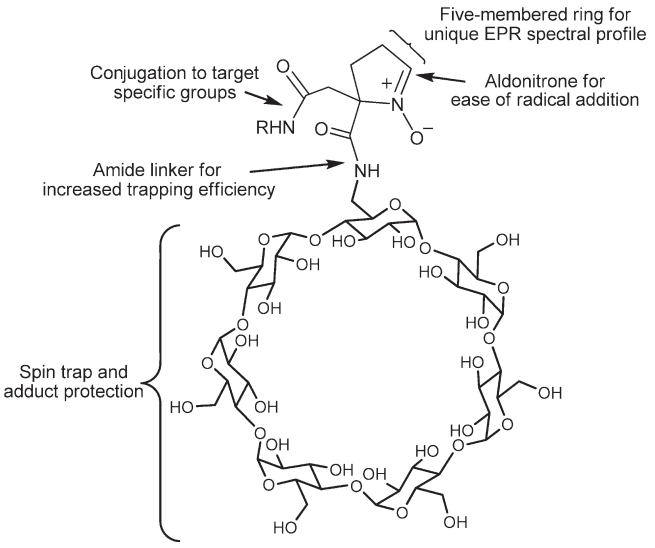

FIGURE 2. Representation of a unified design using a bifunctionalized spin trap.

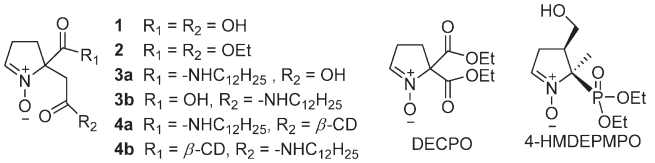

FIGURE 3. Structures of bifunctional cyclic nitrones.

compartments, the aim to achieve high reactivity to $O_2^{\bullet -}$, longer adduct half-life, enhanced bioavailability, and selective targeting in a unified molecular design has been a challenge (Figure 2). These challenges can perhaps be overcome through synthesis of a novel dicarboxylated cyclic nitrone **1** (Figure 3) that can be conjugated via amide bond to various groups for enhanced adduct stability and bioavailability. With the expectation that a β-CD group would lead to persistent spin adduct while a lipophilic chain may impart membrane affinity, we synthesized and demonstrated the spin trapping properties of **1** conjugated to a β-CD and dodecyl chain.

Results and Discussion

Synthesis. Only a few cyclic nitrone analogues with bifunctional groups have been synthesized over the past years, such as **DECPO**[38] and 5-diethoxyphosphoryl-4-hydroxymethyl-5-methyl-1-pyrroline-*N*-oxide, 4-HMDEPMPO[39] (Figure 3). While **DECPO** may offer opportunities for biconjugation via an amide bond, we have not been successful in hydrolyzing **DECPO** to a dicarboxylic acid nitrone due to the decarboxylation reaction that occurs during base hydrolysis. In order to resolve this problem, compound **2** (see Figure 3 and Scheme 1) was designed to have an extra methylene group on one of the substituents at the C-5 position, which could be hydrolyzed successfully to dicarboxylic acid cyclic nitrone (Scheme 1).

Nitrodiethyl ester **7** was prepared by alkylation of the nitroester **6** with bromoester **5** using $KHCO_3$ and tetrabutylammonium bromide as base and phase transfer catalyst, respectively, according to the published procedures.[40] Purification of compound **7** by column chromatography gave 46% yield. Michael addition of acrolein to the nitrodiester **7** led to compound **8**, which was immediately used without further purification. Reductive cyclization of **8** using Zn/NH_4Cl[41] gave the nitrone **2** after purification. Compound **2** was then subjected to base hydrolysis of the ester bond then followed by ion exchange column chromatography to give **1** as a slightly yellowish solid.

The presence of carboxylic acid functional groups in **1** allows conjugation to a dodecyl group via amide bond, however, without any expectation of regioselectivity during the grafting. In order to avoid disubstitution of **1** by the dodecyl group, equimolar amounts of dodecylamine and **1** were used for the coupling step. As expected, a mixture of the two monosubstituted nitrones **3a** and **3b** was obtained, but evidence of formation of the disubstituted analogue was not investigated as only the polar fractions in the preparative TLC were isolated. However, the low yield of **3a** and **3b** suggests that biconjugation of the dodecyl group also occurs. Due to similarities in the structure and polarity of **3a** and **3b**, chromatographic separation of the mixture using preparative TLC was not successful. As shown in Figure S9 in the Supporting Information, the ^{1}H NMR spectrum of the mixture shows the presence of relevant moieties such as the alkyl chain at 0.9−1.5 ppm, the pyrroline group with the amido and carboxy methylenes at 2.5−3.4 ppm, and the nitronyl proton at 7.11 ppm. Unfortunately, due to the overlap of the amido and carboxy methylene peaks, we were unable to determine the ratio between **3a** and **3b** based on proton integration. Infrared as well as mass spectrometry analyses were also performed, confirming the structure of nitrones **3a**−**3b** (see Figure S10 and S11 in Supporting Information).

The next step in the synthesis was to graft the β-CD moiety onto the lipophilic nitrones. The coupling of the **3a**−**3b** mixture with the amino-β-CD was performed in the presence of EDC/HOBt, yielding a mixture of nitrones **4a** and **4b** after precipitation in acetone. Purification by reverse-phase preparative HPLC led to pure nitrones **4a** and **4b** as demonstrated by HPLC chromatograms and mass spectrometry spectra (see S12, S13, S14 and S15 in Supporting Information).

Compounds **4a** and **4b** have been successfully synthesized and separated, but attempts to spectroscopically differentiate **4a** from **4b** by ^{1}H and ^{13}C NMR alone was difficult due to the similarities in their spectral profiles. MS/MS analysis of **4a** and **4b** also gave the same fragmentation patterns showing a consecutive loss of ions with m/z = 162 corresponding to a glucopyranoside unit. Also evident from the MS/MS spectra of both **4a** and **4b** is the loss of a m/z = 140 corresponding to [5-(2-amino-2-oxoethyl)-1-pyrroline *N*-oxide]$^{\bullet +}$ fragment (see Figure S16 in Supporting Information). Due to the limited quantity of **4a** and **4b** and their limited

(38) Karoui, H.; Clement, J.-L.; Rockenbauer, A.; Siri, D.; Tordo, P. *Tetrahedron Lett*. **2004**, *45*, 149–152.
(39) Chalier, F.; Hardy, M.; Ouari, O.; Rockenbauer, A.; Tordo, P. *J. Org. Chem*. **2007**, *72*, 7886–7892.
(40) (a) Diez-Barra, E.; de la Hoz, A.; Moreno, A. *Synth. Commun*. **1994**, *24*, 1817–21. (b) Schipchandler, M. T. *Synthesis* **1979**, *9*, 666–686.
(41) Tsai, P.; Elas, M.; Parasca, A. D.; Barth, E. D.; Mailer, C.; Halpern, H. J.; Rosen, G. M. *J. Chem. Soc., Perkin Trans. 2* **2001**, 875–880.

SCHEME 1. Synthetic Scheme for the Bifunctional Cyclic Nitrones 4a and 4b

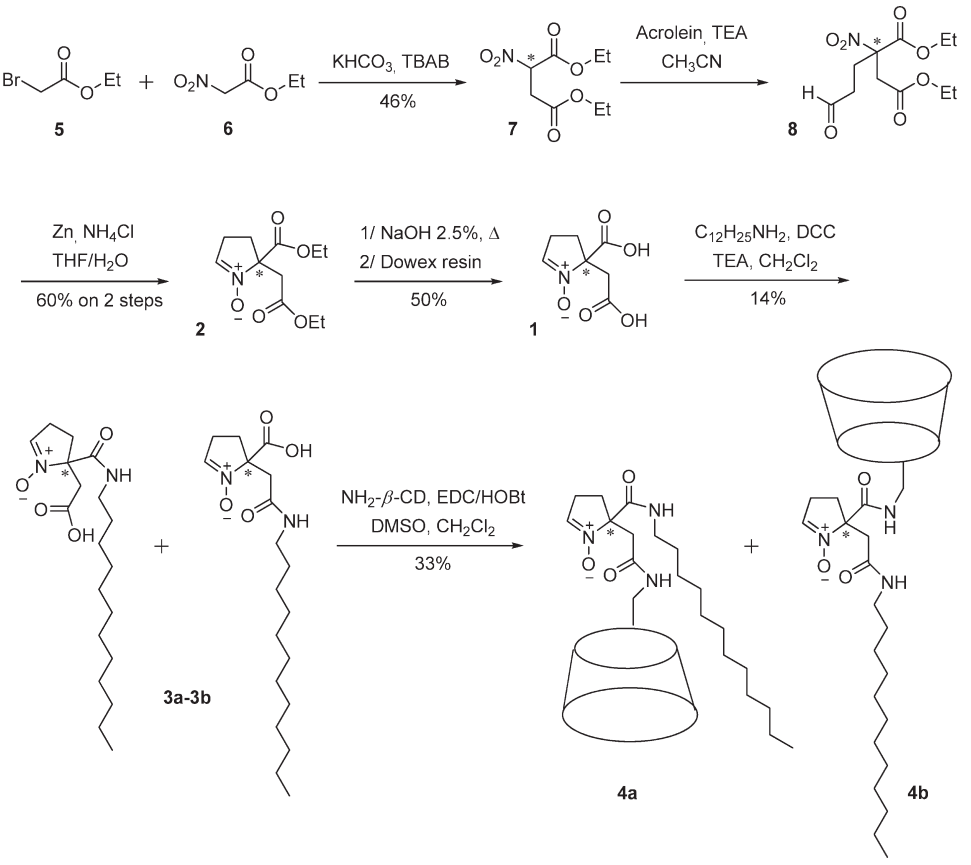

solubility in water or methanol, only an extensive NMR analysis of **4b** using HSQC, TOCSY, HSQC-TOCSY, and HMBC was performed in DMSO-d_6 (see Figures S17−S22 in Supporting Information). The HSQC experiment allowed us to identify the resonance peak of the three methylene protons of interest not originating from the pyrroline ring: (a) an AB system at 2.60−2.85 ppm; (b) a multiplet at 2.98 ppm; and (c) a doublet at 3.45 ppm that is overlapping with the β-CD peaks (see Figure 4), with corresponding ^{13}C resonance peaks at 39.5, 38.4, and 40.4 ppm, respectively. Fortunately, TOCSY and HSQC−TOCSY experiments allowed us to assign the 2.98 ppm peaks to the first methylene protons of the dodecyl group that is attached to the amide nitrogen (labeled as (b) protons in Figure 4). Since no correlation between the protons of the AB system (i.e., the (a) protons) and any other protons was observed from TOCSY or HSQC−TOCSY, this suggests that the (a) protons are those of the methylene group attached to the pyrroline ring. The next step is to precisely assign which methylene group (i.e., either from the β-CD or from the dodecyl) is connected to the (a) protons via the amide bond. As shown in Figure 4, the HMBC experiment provided useful information regarding the connectivity in the molecule. The (a) protons gave long-range coupling with the carbon of the dodecyl group that is attached to the amide nitrogen (i.e., the (b) protons) as well as with the carbonyl carbon(I) at 167.4 ppm. Although a long-range correlation between (a) protons and the other carbonyl carbon(II) at 169.4 ppm was also observed due to their proximity to one another, no correlation was observed between the (b) protons and the other carbonyl carbon(II) at 169.4 ppm. This clearly demonstrates that the (b) protons are closer to the (a) protons than to the (c) protons, as shown in Figure 4. Also worth noting are the two amide triplet peaks at 7.86 and 8.58 ppm, which are correlated to the carbonyl carbons, I and II, respectively (Figure 4). The amide hydrogen at 7.86 ppm shows strong correlation with the (b) and (a) protons but only a weak correlation with (c) protons, while the amide hydrogen at 8.58 ppm shows stronger correlation with (c) and (a) but not with (b), further demonstrating the correct connectivity assignments for **4b**.

NMR and Inclusion Studies. A detailed structural analysis of β-CDMPO was described in our previous paper.[24] Figures S23a and S23b in Supporting Information show similarities between the ROESY spectra of **4a** and **4b** in D_2O, respectively. Unlike in DMSO, the ^1H NMR spectrum is more complex in D_2O due to the presence of extensive H-bonding resulting in the formation of distinctive conformational isomers for **4a** and **4b**. The presence of various conformational isomers for **4a** and **4b** was studied computationally and will be discussed in detail in the succeeding section. Only weak correlation of cyclic nitrone with β-CD can be observed. However, a strong long-range correlation can be observed from the dodecyl group interaction with the β-CD cavity, and this is more pronounced for **4b** than in **4a**. This difference in the degree of interaction between the dodecyl group with the hydrophobic core of the β-CD in **4b** and **4a** could be due to the presence of the extra methylene group separating the nitrone and the dodecyl moiety in **4b**, providing more flexibility for the dodecyl group for interaction with the β-CD.

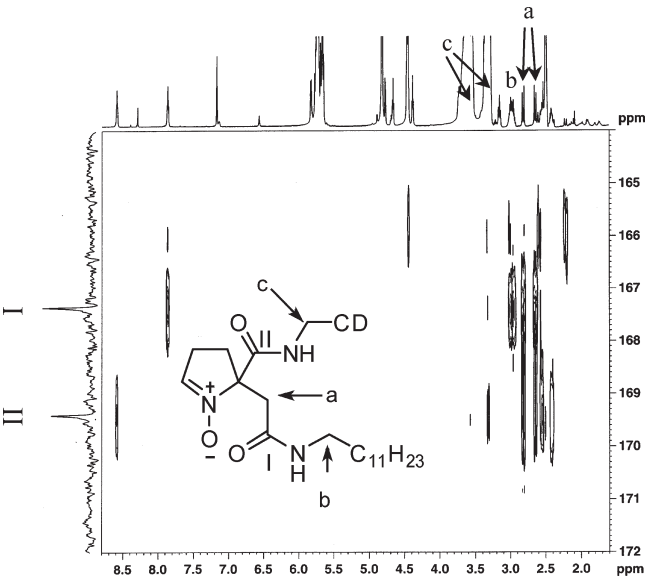

FIGURE 4. $^1H-^{13}C$ HMBC spectra (600 MHz) of **4b** in DMSO-d_6 showing the three methylene groups (a, b, and c) of interest and their long-range correlation with the two carbonyl carbons (I and II).

Furthermore, in order to explore the inclusion properties of **4a** and **4b**, L-borneol was used as a competitor guest molecule.[24] Ordinarily, L-borneol will displace the included moiety in β-CD due to the strong inclusion complex formed by L-borneol with β-CD. As shown in Figures S23c and S23d in Supporting Information, the ^1H NMR peaks of **4a** and **4b** are shifted and broader with the addition of L-borneol. For example, the peaks at ~5.0 and 3.5−4.0 ppm that are assigned to β-CD-H's were shifted downfield to ~5.3 and 3.8−4.3 ppm, respectively, while the peaks at 1.1−1.5 ppm that are assigned to the dodecyl-H's were shifted upfield to ~1.1 ppm. Worth noting is the disappearance of the correlation between β-CD and dodecyl-H's, but interestingly, the correlation between β-CD and l-borneol was not apparent due perhaps to the fast exchange between L-borneol and the dodecyl group, as evidenced by the broadened ^1H NMR spectra of **4a** and **4b** in the presence of L-borneol. Also, the area of the correlation peaks for β-CD and the dodecyl group in **4b** is bigger compared to that in **4a**, indicating that there could be more inclusion isomers in **4b** than in **4a**. It should be noted, however, that the area of correlation peaks observed between the protons of β-CD and dodecyl group for both **4a** and **4b** is minor relative to the total peak area observed for the ^1H NMR spectra of the dodecyl protons at the 1−2 ppm region (Figures S23a and S23b in Supporting Information), suggesting that an inclusion complex may not be the only conformation present in solution.

Induced Circular Dichroism (ICD). To give more insights into the nature of β-CD and dodecyl group interaction, ICD measurements were carried out. As shown in Figure S24 in Supporting Information, **1** gave no ICD band as expected for a racemic mixture. However, **4a** and **4b** show minima at 220 and 205 nm, respectively, while the same maxima at 243 nm can be observed for both isomers (Figure 5). The observed optical activity for **4a** and **4b** in spite of the presence of racemates could be due to the effect of the intrinsic chirality of β-CD on the orientation or conformation[42] of the nitrone group thereby exhibiting ICD bands. The high intensity bands suggest strong intramolecular interaction of the nitrone chromophore with the β-CD. The difference in the minima between **4a** and **4b** suggests that the nitrone moiety in these two isomers may exhibit different spatial orientation in solution, consistent with their ROESY spectra and will be further demonstrated by spin trapping studies and particle size analysis in the succeeding sections. Moreover, concentration dependence study of the ICD spectra of **4a** and **4b** (Figure 5) shows direct correlation of the band intensity at 243 nm with decreasing concentration. This result suggests that the conformations of **4a** and **4b** are not affected by concentration; otherwise, a nonlinear curve at the same concentration range similar to those previously reported should be observed.[43]

Self-Aggregation Properties. The self-aggregation properties in water of pure β-CDs have been extensively investigated for 15 years. Coleman reported[44] the formation of β-CD aggregates with an average diameter of around 200 nm that might be rod-like aggregates, while Gonzáles-Gaitano et al.[45] observed the formation of ~300 nm diameter size clusters. More recently, Baglioni and co-workers[46] demonstrated the formation of aggregates with 190 nm diameter. Cyclodextrins bearing additional groups that are either hydrophilic or hydrophobic have been found to exhibit more pronounced self-aggregation properties than pure CDs, leading to well-characterized supramolecular aggregates (e.g., spherical micelles[47,48] or vesicles).[49]

The self-aggregation properties of compounds **4a** and **4b** were investigated by dynamic light scattering (DLS) technique at a concentration range of 1 to 0.1 mM, and the results are expressed as volume distribution percentage as shown in Table 1.

Both **4a** and **4b** self-organize in water into particles with apparent hydrodynamic diameters that are within the range of ~100 to 300 nm but are not in agreement with the formation of spherical micelles. This first observation tends to suggest that cyclodextrin derivatives cannot be considered as classical surfactants. Indeed, recent reports showed that C12 surfactants bearing bulky glucose-based polar heads lead to the formation of spherical micelles of 5.2 nm diameter.[50] Smaller particles of ~60 nm diameter were also observed with compound **4b** but not within the whole concentration range mentioned above. These smaller aggregates

(42) (a) Hamilton, J. A.; Chen, L. *J. Am. Chem. Soc.* **1988**, *110*, 5833–5841. (b) Tanaka, M.; Shono, T.; Zhu, D.; Kawaguchi, Y. *J. Chromatogr.* **1989**, *469*, 429–433.

(43) Park, J. W.; Song, H. E.; Lee, S. Y. *J. Org. Chem.* **2003**, *68*, 7071–7076.

(44) Coleman, A. W.; Nicolis, I.; Keller, N.; Dalbiez, J. P. *J. Inclusion Phenom.* **1992**, *13*, 139–143.

(45) (a) Gaitano, G. G.; Brown, W.; Tardajos, G. *J. Phys. Chem. B* **1997**, *101*, 710–719. (b) González-Gaitano, G.; Rodríguez, P.; Isasi, J. R.; Fuentes, M.; Tardajos, G.; Sánchez, M. *J. Inclusion Phenom.* **2003**, *44*, 101–105.

(46) (a) Bonini, M.; Rossi, S.; Karlsson, G.; Almgren, M.; Lo Nostro, P.; Baglioni, P. *Langmuir* **2006**, *22*, 1478–1484. (b) Rossi, S.; Bonini, M.; Lo Nostro, P.; Baglioni, P. *Langmuir* **2007**, *23*, 10959–10967.

(47) Auzely-Velty, R.; Djedaini-Pilard, F.; Desert, S.; Perly, B.; Zemb, T. *Langmuir* **2000**, *16*, 3727–3734.

(48) Mazzaglia, A.; Ravoo, B. J.; Darcy, R.; Gambadauro, P.; Mallamace, F. *Langmuir* **2002**, *18*, 1945–1948.

(49) (a) Ravoo, B. J.; Darcy, R. *Angew. Chem., Int. Ed.* **2000**, *39*, 4324–4326. (b) Ravoo, B. J.; Jacquier, J.-C.; Wenz, G. *Angew. Chem., Int. Ed.* **2003**, *42*, 2066–2070.

(50) Abla, M.; Durand, G.; Pucci, B. *J. Org. Chem.* **2008**, *73*, 8142–8153.

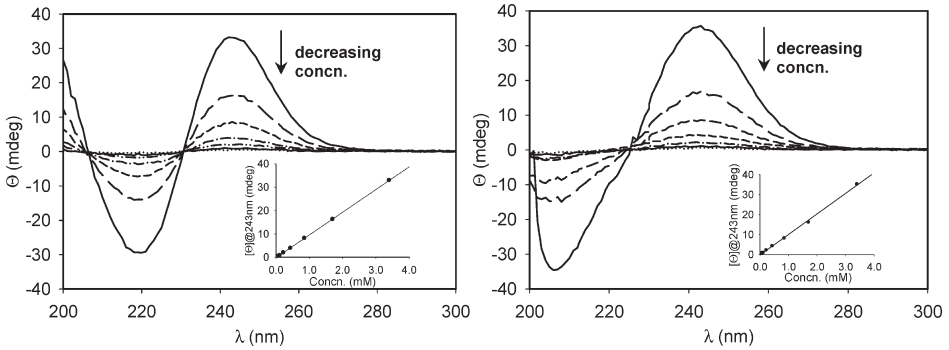

FIGURE 5. Concentration dependence of ICD spectra of **4a** (left) and **4b** (right). The concentrations of **4a** or **4b** from bottom to top at 243 nm are 0.06, 0.11, 0.22, 0.43, 0.85, 1.70, and 3.40 mM. The inset shows the dependence of the ellipticity at 243 nm on the concentration of **4a** or **4b**.

TABLE 1. Particle Size Distribution Parameters by DLS in Aqueous Solution at 25 °C

	4a			4b		
concn	D_H[a]	HHW[b]	PDI[c]	D_H[a]	HHW[b]	PDI[c]
1 mM	132 ± 27	12 ± 3	0.761	71 ± 12 (20%)[d]	11 ± 3	0.517
				267 ± 49 (66%)[d]	34 ± 7	
0.5 mM	174 ± 35	16 ± 3	0.612	58 ± 25 (64%)[d]	12 ± 3	0.478
				166 ± 28 (21%)[d]	30 ± 11	
0.1 mM	128 ± 51	11 ± 5	0.786	171 ± 10 (29%)[d]	18 ± 2	0.17
				290 ± 9 (71%)[d]	32 ± 1	

[a] D_H: hydrodynamic diameter of particles in nanometers. The values reported are average of 14 measurements. [b] HHW, the width of the peak at half-height, an indication of the degree of polydispersity of the aggregates. [c] PDI, polydispersity index. [d] Percentage of volume distribution.

could be micellar aggregates as previously demonstrated with amphiphilic β-CD compounds.[29,48] However, these smaller particles were in equilibrium with two types of aggregates, that is, one at around 170−270 nm and one at 2600 nm (not reported in the table, with percent volume distribution less than 15%). During the course of the experiment with **4a**, similar aggregates were also observed but were less persistent. Moreover, the aggregates of **4a** exhibit a lower polydispersity than that of **4b**, as shown by the half-height width (HHW) and polydispersity index (PDI). This confirms the different behavior of **4a** and **4b** in aqueous solution as demonstrated above by NMR and circular dichroism. Also, the reproducibility of the size distribution of aggregates in independently prepared samples was found to be slightly variable. Hence, the first experimental trial with **4a** did not allow us to observe persistent large aggregates, but these aggregates were observed in the second trial, however, with a volume distribution below 25% (data not shown), indicating the dynamic nature of this aggregation process.

Transmission Electron Microscopy. Imaging of the aggregate morphologies formed from **4a** was possible and is shown in Figure 6. High density of spherical aggregates with a diameter of 20−50 nm was observed 30 min after dissolution of **4a** in water. When the solution was allowed to stand for 2 h, spherical aggregates of a larger diameter of ∼100 nm were observed while the density of the small aggregates was decreased. This confirms the occurrence of a dynamic equilibrium, as observed by DLS, and suggests that the small aggregates formed immediately after the dispersion in water may coalesce to form bigger ones. None of the particles

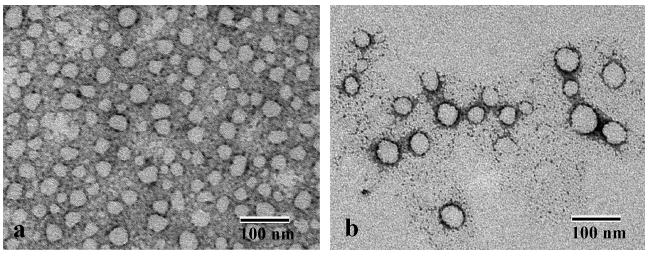

FIGURE 6. Electron micrographs of **4a** solution (2 mM) in water (a) 30 min and (b) 2 h after sonication.

observed showed dark centers that could originate from an aqueous core, indicating the formation of vesicles. Only disk-like morphology was observed, suggesting the formation of nanoparticles but with no precise evidence of their composition.

EPR Spin Trapping Studies. Compound 1. The spin trapping properties of **1** for $HO^{\bullet}$ and $O_2^{\bullet-}$ were investigated. Hydroxyl radical was generated using Fenton reaction, while $O_2^{\bullet-}$ was produced using the xanthine/xanthine oxidase system in phosphate buffer. As shown in Figure S25 in Supporting Information, **1** gave an EPR signal with $HO^{\bullet}$ but not with $O_2^{\bullet-}$ using the same nitrone concentration. This phenomenon is similar to that observed by Rosen et al.,[41] although the mechanism for this observation is still unclear, but we hypothesize that this could be due to the repulsion between the negatively charged carboxylate anion and $O_2^{\bullet-}$/$HO_2^{\bullet}$ or perhaps the dismutation of $O_2^{\bullet-}$ in the presence of exchangeable protons competing with the spin trapping reaction.

Compounds 4a and 4b. Although the β-CDMPO alone in the absence of hydrophobic dodecyl group gave a robust EPR signal upon trapping $O_2^{\bullet-}$ in an aqueous system,[24] generation of $O_2^{\bullet-}$ in an aqueous system with **4a** or **4b** (20 mM) only gave a weak EPR signal (data not shown) due probably to the formation of an aggregate or formation of a conformation that may shield the nitrone from the radicals. However, the EPR signal was stronger when $O_2^{\bullet-}$ spin adducts of **4a** and **4b** were generated in DMSO at the same concentrations (Figure 7). On the basis of the spectra shown in Figure 7, $O_2^{\bullet-}$ adducts exhibited hindered molecular tumbling as characterized by smaller magnitude and broadening of the highest-field line compared to the lowest-field line. These partial anisotropic behaviors may be due to the relatively large size of the molecules, solvent viscosity, and/or dipolar interaction. The EPR

TABLE 2. EPR Parameters for the Hydroxyl and Superoxide Radical Anion Adducts of 4a and 4b in DMSO

Hydroxyl Adducts (in PBS)						
				relaxation coefficients[a]		
adducts	g	a_N (G)	$a_{\beta\text{-H}}$ (G)	α	β	γ
4a-OH[a]	2.0054	13.8	12.7	1.82	0.41	0.46
4b-OH	2.0053	13.8	12.5	1.77	0.38	0.38

Superoxide Adducts (in DMSO)[b]					
	axis	g	a_N (G)	$a_{\beta\text{-H}}$ (G)	correlation time (ns)
4a-OO^-	x	2.0089	2	12	1.74 (**4a**)
or	y	2.0085	3	10	
4b-OO^-	z	1.992	31	11	1.61 (**4b**)

[a] $\Gamma = \alpha + \beta M_I + \gamma M_I^2$, where Γ is the line width, α, β, and γ are relaxation coefficients, and M_I is the z component secondary quantum number for the nuclear spin angular momentum for N atom ($M_I = 1$). [b] The anisotropic g's, hfsc's, and correlation times were calculated as follows: From the isotropic signal, the line width variation was interpreted via a relaxation model assuming a rhombic g and hyperfine tensors, where the anisotropy was partially averaged out by the isotropic rotational tumbling. The spectrum fit was optimized for both the anisotropic tensor elements and the correlation time.

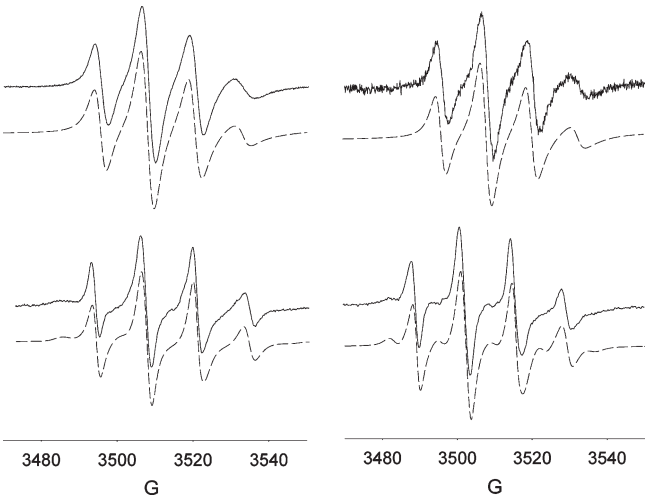

FIGURE 7. X-band EPR spectra of the superoxide radical anion and hydroxyl adducts of **4a** and **4b** (20 mM) generated using KO_2/DMSO and Fe^{2+}/H_2O_2 in PBS, respectively. Simulated spectra are shown as trace plots. EPR isotropic and anisotropic parameters are shown in Table 2, and experimental conditions are described in the text.

parameters for $O_2^{\bullet-}$ adducts are shown in Table 2 and gave higher correlation time for **4a**-$O_2^{\bullet-}$ adduct compared to the **4b**-$O_2^{\bullet-}$ adduct, indicating a more restricted molecular motion for the former. However, due to the significant anisotropy in the spectra observed for the $O_2^{\bullet-}$ adducts, the percent population of the isomers cannot be determined. The calculated angle between the slow rotation axis and the magnetic z-axis is around 60° for the $O_2^{\bullet-}$ adducts.

The EPR spectra of the $HO^\bullet$ adducts in aqueous solution obtained from Fenton reaction using 20 mM of **4a** or **4b** are shown in Figure 7. Unlike in the formation of $O_2^{\bullet-}$ adducts from **4a** and **4b** in aqueous solution, the $HO^\bullet$ adducts gave a relatively more robust signal in water in spite of their tendency to aggregate in an aqueous system. As shown in Table 2, there is a difference in relaxation coefficients between **4a**-OH and **4b**-OH, in which the former shows a more hindered molecular tumbling motion than the latter. This observation is consistent with our results from NMR, ICD, and DLS studies, suggesting a higher equilibrium concentration of the inclusion form for **4b** compared to **4a**, further confirming the difference in the conformation between **4a** and **4b** and their respective $O_2^{\bullet-}$ and $HO^\bullet$ adducts. Due to the higher presence of non-included dodecyl chain in **4a** and its adducts, it can be assumed that these may give a more pronounced surfactant-like behavior compared to **4b**. The extra methylene group that connects the nitrone moiety and the dodecyl group in **4b** could allow formation of an inclusion complex more facile than in **4a**. Finally, since **4a** and **4b** gave a similar spectral profile for $HO^\bullet$ and $O_2^{\bullet-}$, using a mixture of **4a** and **4b** for spin trapping applications should not limit spectral interpretation.

Kinetics of $O_2^{\bullet-}$ Adduct Formation and Decay. Due to the poor spin trapping ability of **4a** for $O_2^{\bullet-}$ in an aqueous system, kinetic studies were performed in DMF solution using stopped-flow kinetics as previously described.[13,51] Figure 8 shows the kinetic plots for the reaction of **4a**, DMPO, and β-CD with KO_2 and gave $k_{\mathbf{5a}}/k_{PR}$, k_{DMPO}/k_{PR}, and $k_{\beta\text{-CD}}/k_{PR}$ of 5.17, 0.04 (lit. 0.02),[51] and 0.30, respectively, indicating that **4a** is ~130 times more reactive to $O_2^{\bullet-}$ than DMPO. Surprisingly, β-CD alone exhibits reactivity toward $O_2^{\bullet-}$ and is ~ 7.5 times more reactive than DMPO. The nature of $O_2^{\bullet-}$ reactivity to β-CD could be due to the α effect similar to those observed for $O_2^{\bullet-}$ interaction with amino acids and non-amino acids bearing H-bond donors.[52] On the basis of the absolute second-order rate constant for DMPO of 1.7 M^{-1} s^{-1} obtained[13] using stopped-flow kinetics, the rate constant for $O_2^{\bullet-}$ trapping by **4a** can be estimated to be 221 M^{-1} s^{-1}, which is considerably faster compared to other substituted cyclic nitrones[13] such as AMPO (135 M^{-1} s^{-1}), EMPO (104 M^{-1} s^{-1}), and DEPMPO (0.65 M^{-1} s^{-1}) and linear nitrones (0.13−0.80 M^{-1} s^{-1})[51] whose rate constants were obtained using the same experimental conditions as **4a**. Although **4a** shows poor reactivity to $O_2^{\bullet-}$ in aqueous solution due to the possible formation of aggregates, this improved reactivity to $O_2^{\bullet-}$ in nonpolar systems can be potentially applied to scavenge $O_2^{\bullet-}$ in lipid membranes.

The decay kinetics of $O_2^{\bullet-}$ adducts of various spin traps were also explored to investigate the effect of the β-CD moiety on the stability of **4a**. The various $O_2^{\bullet-}$ adducts were generated in DMSO using 2 mM spin trap and KO_2 (see Experimental Section for details), and the half-lives based on first-order decay kinetics were calculated as follows (in min): DMPO-O_2H (3.6 ± 0.7), DEPMPO-O_2H (2.4 ± 0.3); AMPO-O_2H (2.6 ± 0.2); β-CDMPO-O_2H (5.7 ± 1.1); and **4a**-O_2H (9.0 ± 2.8). Results show that the half-life for the

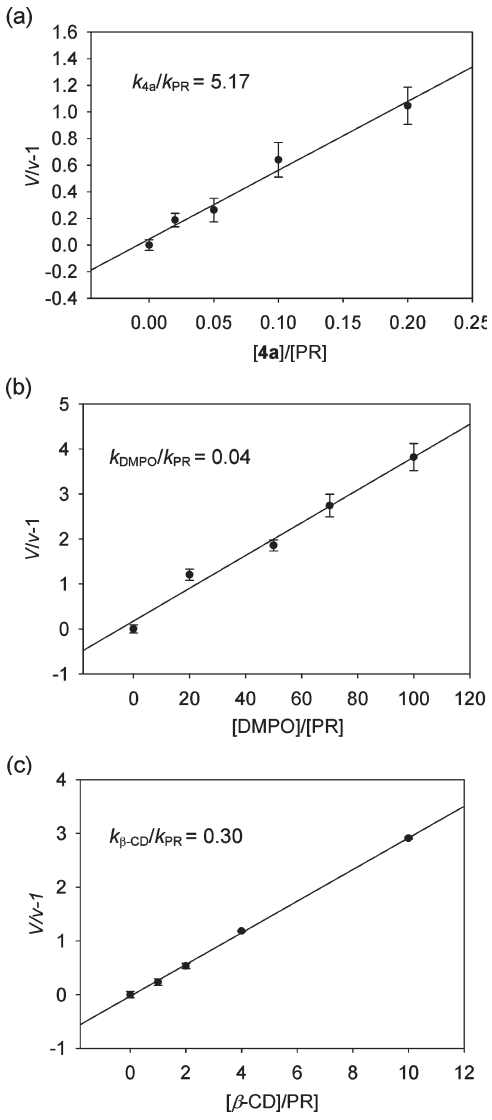

FIGURE 8. Stopped-flow kinetic plots of (a) **4a**, (b) DMPO, and (c) β-CD for their reaction with KO_2 in DMF using phenol red (PR) as competitor, where V and v are the initial rates of formation in the absence and presence of various concentrations of the spin trap, respectively. Initial rates were obtained by monitoring the formation of a UV−vis absorption peak at 575 nm. Measurements were done at least in triplicate. See Experimental Section for details.

$O_2^{\bullet-}$ adduct of DMPO is longer (3.6 min) compared to 1 min in aqueous solution, consistent with that previously reported[53] for the decay of DMPO-O_2H in aprotic solvents. However, the $O_2^{\bullet-}$ adducts of DEPMPO, AMPO, and β-CDMPO in DMSO are considerably shorter compared to that found in an aqueous system of 14,[54] 8,[14] and 28 min,[24] respectively. This discrepancy could be due to the annihilation of the intramolecular H-bond interaction in DMSO, which is believed to be mostly responsible for adduct stability.[14,19,24,55] Nevertheless, this work only aims to give a qualitative trend on the relative stability of the adducts and to demonstrate how conjugation of a β-CD group to nitrones can enhance $O_2^{\bullet-}$ adduct stability as shown by the higher $t_{1/2}$ for β-CDMPO-O_2H and **4a**-O_2H compared to the nonconjugated nitrones.

Molecular Modeling of 4a,b and Their $O_2^{\bullet-}$ Adducts. In order to investigate the effects of conformation as well as stereoisomerism on the stability of **4a**,**b** and their corresponding $O_2^{\bullet-}$ adducts, computational studies were carried. Table S1 in Supporting Information shows the calculated relative bottom-of-the-well energies of the various isomers of **4a** and **4b**. Two conformational isomers can be seen in Figure 9 for the (5*R*)-**4b** isomer in which the dodecyl group is outside the β-CD cavity and is more thermodynamic favorable compared to when the dodecyl group is inside. Similar observation can be seen for (5*S*)-**4a** but only gave ~6 kcal/mol energy difference between the self-included and excluded conformations (Figure S27 in Supporting Information). However, the reverse is true for (5*R*)-**4a** and (5*S*)-**4b**. These differences in the preferred conformations (i.e., included and excluded) could be due to the orientation of the nitrone moiety relative to the β-CD annulus. Careful examination of the orientation of the nitrone group shows that the N−O points directly toward the β-CD annulus in the lower energy isomers compared to the higher ones in which the N−O points away from the β-CD annulus (see Figure 9 and Figures S27 and S28 in Supporting Information). The preferred conformations show the N−O moiety exhibiting a strong intramolecular H-bonding interaction with the hydroxyl H of the β-CD. This indicates that the orientation of the nitrone relative to the β-CD annulus is strongly influenced by the stereochemistry around C-5 and the constitutional isomerism of **4**. Therefore, the interaction of the nitrone with the β-CD plays a more important role in the conformational stability of **4** than the position of the dodecyl group (i.e., whether included or excluded). The presence of H-bond interaction between the amide-H and β-CD-OH's might also be a contributing factor to the stability of the conformation, but this was also observed in the least stable isomers.

The effect of isomerism on the stability of various $O_2^{\bullet-}$ adducts of **4a** and **4b** was also investigated, and Table S1 in Supporting Information shows the relative bottom-of-the-well energies for these adducts. Similar to that observed for **4a** and **4b**, the preferred conformation is characterized by intramolecular H-bond interaction of the nitronyl O and hydroperoxyl H with the β-CD-OH's. For example as shown in Figure S29 in Supporting Information, (2*R*,5*R*)-**4b**-OOH (excluded) gave the most preferred conformation in which intramolecular H-bond interaction of the aminoxyl O and hydroperoxyl H with the β-CD-OH's is evident followed by (2*S*,5*R*)-**4b**-OOH (excluded) in which only the aminoxyl O shows intramolecular interaction with β-CD-OH and not the hydroperoxyl H. Both the included isomers (2*S*,5*R*)-**4b**-OOH and (2*R*,5*R*)-**4b**-OOH are least preferred and both the N−O and −OOH groups show no direct interaction with the β-CD-OH's (see Figure S29 in Supporting Information). In general, for (5*S*)-**4b**-OOH, (5*R*)-**4a**-OOH, and (5*S*)-**4a**-OOH

(51) Durand, G.; Choteau, F.; Pucci, B.; Villamena, F. A. *J. Phys. Chem. A* **2008**, *112*, 12498–12509.
(52) Field, S. M.; Villamena, F. A. *Chem. Res. Toxicol.* **2008**, *21*, 1923–1932.
(53) Roubaud, V.; Lauricella, R.; Tuccio, B.; Bouteiller, J.-C.; Tordo, P. *Res. Chem. Intermed.* **1996**, *22*, 405–416.
(54) Tuccio, B.; Lauricella, R.; Frejaville, C.; Bouteiller, J.-C.; Tordo, P. *J. Chem. Soc., Perkin Trans. 2* **1995**, 295–298.
(55) Villamena, F. A.; Merle, J. K.; Hadad, C. M.; Zweier, J. L. *J. Phys. Chem. A* **2005**, *109*, 6083–6088.

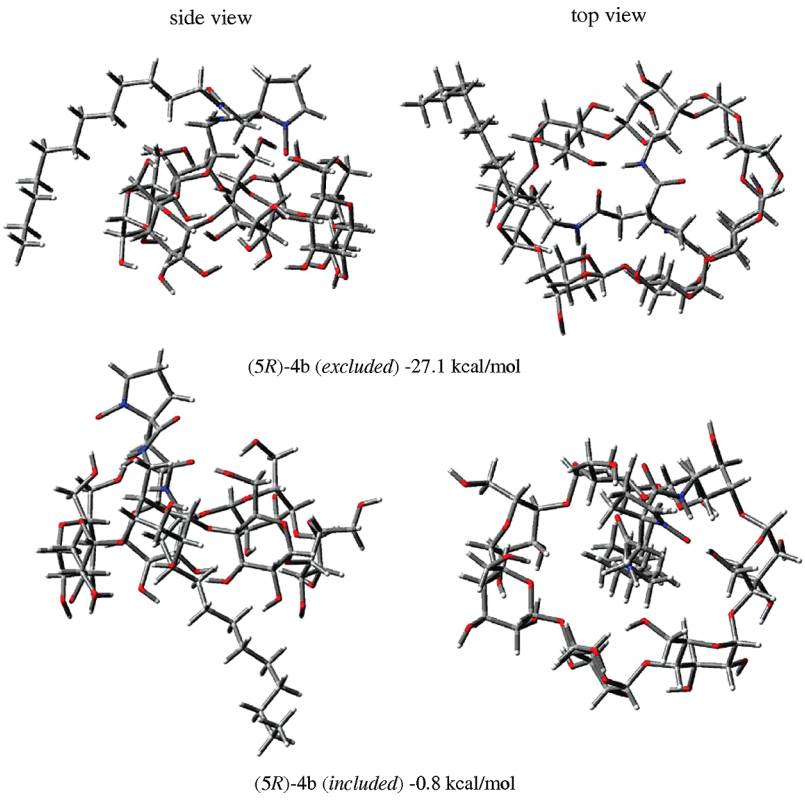

FIGURE 9. Side and top views of the optimized geometries of **4b** at the HF/3-21G* level of theory showing the dodecyl group outside (top) and inside (bottom) the β-CD cavity and their relative bottom-of-the-well energies.

isomers, a similar trend was observed in which the most preferred adducts show H-bond interaction of the N−O and −OOH moieties with β-CD-OH's (see Table S1 and Figures S29−S32 in Supporting Information). Therefore, the orientations of N−O and −OOH relative to the β-CD annulus are also strongly influenced by the stereochemistry around C-2 and C-5 as well as the constitutional isomerism in **4**.

The complex formed between **4a**/**4b** and the guest molecule, borneol, was also computationally investigated. Table S1 in Supporting Information shows the relative bottom-of-the-well energies for the various conformations of the **4a**/**4b**···borneol complex. Results show that the location of the borneol being on the opposite side of the β-CD annulus relative to the nitrone group is more preferred than when the borneol and the nitrone groups are on the same side of the annulus, such as in the case of (5*R*)-**4b** (see Figure S33 in Supporting Information). This observation could be due to the repulsive effect between the nitrone group and borneol being on the same side of the annulus. Conversely, the borneol being on the other side of the nitrone group maximizes the intramolecular H-bonding between the nitrone and β-CD as the borneol does not compete for the H-bonding sites. The same trend is observed for (5*S*)-**4b** (Figure S34 in Supporting Information). In the case of (5*R*)-**4a** and (5*S*)-**4a** (Figures S33 and S34 in Supporting Information, respectively), the presence of an extra methylene group between the nitrone and β-CD gives the nitrone more freedom to reduce the repulsion with borneol, although they are both in the same side of the annulus, and therefore does not follow the same observation as in (5*R*)-**4b** and (5*S*)-**4b** (Figures S33 and S34 in Supporting Information, respectively).

Conclusions

Bifunctionalization of cyclic spin trap with β-CD and a lipophilic dodecyl chain using amide linkers gave two structural racemic isomers, **4a** and **4b**, which were unequivocally characterized by 1-D, 2-D homo- and heteronuclear NMR, as well as MS and MS/MS experiments. Circular dichroism and ROESY coupled with competition experiments with borneol suggest that the nitrone and dodecyl group interaction with the β-CD is intramolecular in nature. DLS and TEM show that these compounds self-aggregate in aqueous solution and form particles with sizes ranging from 100 to 300 nm. Spin trapping of $O_2^{\bullet-}$ by **4a** and **4b** in DMSO is more favored than in aqueous solution, suggesting that the self-aggregation plays a crucial role in the spin trapping property of the biconjugated nitrone. The kinetics of formation and decay of $O_2^{\bullet-}$ adducts of **4a** in aprotic polar solvents gave increased rate of spin trapping and longer adduct decay compared to the commonly used spin traps and β-CDMPO. Computational analysis of **4a** and **4b** preferred structures shows strong intramolecular H-bond interaction of the nitronyl NO group with the β-CD-OH's on the annulus. Moreover, the preferred conformations for the **4a/4b-OOH** adducts were computationally rationalized. Similar to **4a**/**4b** alone, the preferred conformations for the adducts are influenced by both constitutional and stereochemical isomerism that allows optimal intramolecular H-bond interaction between the aminoxyl NO and the hydroperoxyl H with

the β-CD-OH's on the annulus. Efforts are now underway to conjugate β-CDMPO to other groups that are target specific to cellular compartments such as the mitochondria, cytosol, and extracellular matrix.

Experimental Section

Synthesis. (a) 5-(2-Ethoxy-2-oxoethyl)-5-(ethoxycarbonyl)-1-pyrroline *N*-oxide (2). The synthesis of diethyl 2-nitrosuccinate (**7**) was carried out according to published procedures,[40] and its spectral data were in agreement with the literature.[40] TEA (0.2 mL) was slowly added to a cooled (10 °C) solution of **7** (1.8 g, 8.2 mmol) and acrolein (0.66 mL, 9.9 mmol) in CH_3CN (5 mL). The mixture was stirred for 2 h at room temperature and then concentrated in vacuo to give the crude product **8**. The crude product **8** was dissolved in THF (90 mL) at −10 °C, and a solution of NH_4Cl (2.8 g) in 20 mL of water was added followed by Zn dust (2 g), which was added portion-wise within 0.5 h at −10 °C. The mixture was stirred for another 2 h at −10 °C, and solid NaCl was added and extracted with Et_2O. The collected organic phase was dried over anhydrous $MgSO_4$ and filtered. The solvent was removed in vacuo, and the residue was purified by flash column chromatography using CH_2Cl_2/MeOH (97:3 v/v) as eluent to give **2** as yellow oil (1.2 g, 60%): ^{1}H NMR (400 MHz, $CDCl_3$) δ 1.29 (overlap of two triplets, 6H), 2.71 (m, 1H), 2.76 (m, 3H), 3.05−3.33 (AB system, 2H), 4.13−4.27 (m, 4H), 6.97 (t, 1H); ^{13}C NMR (100 MHz, $CDCl_3$) δ 14.3, 14.5, 26.9, 30.2, 38.0, 61.3, 63.0, 79.9, 136.3, 169.1, 170.0; IR (neat, cm^{-1}) ν 3440, 2983, 1733, 1586, 1207, 1183, 1076, 1027; GC-MS calcd for $C_{11}H_{17}NO_5$ *m*/*z* 243.1, found 243.0; HRMS calcd for $C_{11}H_{17}NO_5Na$ [M + Na] 266.1004, found 266.0995.

(b) 5-Carboxy-5-(carboxymethyl)-1-pyrroline *N*-oxide (1). To compound **2** (1.2 g) was added 2.5% NaOH (10 mL), then the mixture was refluxed under argon for 1.5 h (at this point, the color of the mixture changed to brown). After cooling, the reaction mixture was passed through Dowex (H^+ form) ion exchange column using water as eluent. The fractions having pH < 4 were collected and concentrated in vacuo and then purified by flash column chromatography using CH_2Cl_2/MeOH (8:2 v/v) as eluent to give **1** as white solid (0.46 g, 50%): ^{1}H NMR (400 MHz, D_2O) δ 2.35−2.70 (m, 2H), 2.76 (m, 2H), 2.95−3.25 (m, 2H), 7.37 (s, 1H); ^{13}C NMR (100 MHz, $CDCl_3$) δ 27.0, 29.7, 37.4, 79.8, 147.2, 171.8, 173.0; IR (neat, cm^{-1}) ν 3087, 2934, 2502, 1715, 1604, 1172; HRMS calcd for $C_7H_9NO_5Na$ [M + Na] 210.0378, found 210.0373.

(c) 5-(Dodecylcarbamoyl)-5-(2-oxo-2((6,6′-deoxy-β-cyclodextrin)methylamino)ethyl)-1-pyrroline *N*-oxide (4a) and 5-(2-(Dodecylamino)-2-oxoethyl)-5-((6,6′-deoxy-β-cyclodextrin)methylcarbamoyl)-1-pyrroline *N*-oxide (4b). To a solution of **1** (40 mg, 0.2 mmol) in CH_2Cl_2 (2 mL) were added DCC (50 mg, 0.24 mmol), dodecylamine (40 mg, 0.2 mmol), and TEA (2 drops) and stirred for 12 h at room temperature. The product was purified using preparative TLC (thickness, 1.0 mm) and CH_2Cl_2/MeOH (8:2 v/v) as eluent to give a mixture of **3a** and **3b** as yellow oil (10 mg, 14%), which was used without further purification: ^{1}H NMR (400 MHz, $CDCl_3$) δ 0.89 (t, 3H), 1.33 (m, 18H), 1.45 (m, 2H), 2.62 (m, 2H), 2.76 (m, 1H), 2.92 (m, 1H), 3.10 (m, 2H), 7.12 (s, 1H); IR (neat, cm^{-1}) ν 3300, 2923, 2853, 1661, 1548; HRMS calcd for $C_{19}H_{34}N_2O_4Na$ [M + Na] 377.2416, found 377.2418. To a solution of **3a**,**3b** (10 mg, 0.03 mmol) in DMSO (2 mL) were added mono-6-deoxy-6-amino-β-cyclodextrin (60 mg, 0.06 mmol), EDC (10 mg, 0.05 mmol), HOBt (3 mg, 0.03 mmol), and TEA (1 drop). The mixture was stirred at ambient temperature for 2 days. Acetone was added to the reaction mixture to give the crude product as a white precipitate. The precipitate was further purified using reverse-phase HPLC (C18 5μ, 150 mm × 22 mm) with gradient elution from 10 to 40% aqueous MeCN at a flow rate of 10 mL/min using 254 nm UV detection. Fractions were collected, and solvents were removed in vacuo to afford the pure nitrones **4a** (7 mg) and **4b** (7 mg) as white solids (total yield 33%). ^{1}H NMR (400 MHz, D_2O) **4b** δ 0.88 (t, 3H), 1.16−1.36 (m, 20H), 2.16 (m, 2H), 2.43 (m, 1H), 2.56 (m, 2H), 2.63 (s, 1H), 2.81 (m, 4H), 3.00−3.40 (m, 4H), 3.50−3.90 (m, 42H), 4.99 (m, 7H), 7.38 (m, 1H); **4a** δ 0.88 (t, 3H), 1.16−1.36 (m, 20H), 2.16 (m, 2H), 2.43 (m, 1H), 2.56 (m, 2H), 2.63 (s, 1H), 2.81 (m, 4H), 3.00−3.40 (m, 4H), 3.50−3.90 (m, 42H), 4.99 (m, 7H), 7.38 (m, 1H); ^{1}H NMR (600 MHz, DMSO-d_6) **4b** δ 0.85 (t, *J* = 6.9 Hz, 3H), 1.23 (br s, 18H), 1.33 (m, 2H), 2.35−2.58 (m, 4H), 2.60−2.85 (AB system, 2H), 2.97 (m, 2H), 3.15 (t, *J* = 9 Hz, 1H), 3.25−3.40 (m, 13H), 3.50−3.80 (m, 27H), 4.38 (t, *J* = 5.6 Hz, 1H), 4.46 (m, 4H), 4.66 (t, *J* = 5.4 Hz, 1H), 4.78 (s, 1H), 4.82 (s, 6H), 5.55−5.80 (m, 13H), 5.83 (d, *J* = 6.6 Hz, 1H), 7.16 (s, 1H), 7.86 (t, *J* = 5.4 Hz, 1H), 8.54 (br s, 1H); ^{13}C NMR (150 MHz, DMSO-d_6) **4b** δ 14.0, 22.1, 25.2, 26.3, 27.1, 28.7, 28.9, 29.0, 31.27, 38.4, 39.4, 40.4, 59.8, 72.0, 72.3, 72.9, 79.4, 81.4, 83.6, 101.5, 101.9, 102.6, 138.5, 167.4, 169.4; MALDI calcd for $C_{61}H_{104}N_3O_{37}$ [M + H] 1470.635, found 1470.674 (**4a**) and 1470.623 (**4b**).

Particle Size Analyses. The hydrodynamic particle size distributions and polydispersity of amphiphilic cyclodextrins at different concentrations were determined using particle size analyzer equipped with a He−Ne laser (λ = 633 nm, 4.0 mW). In a typical experiment, stock solution was prepared by dissolution of the compounds in filtered water (using 0.22 μm filter and water resistivity of 18.2 MΩ·cm) and sonicated for 5 min. The stock solutions were allowed to stand for 1 h, diluted to the appropriate concentrations, then transferred to a plastic cuvette for measurements. Solutions were not filtered. The time-dependent correlation function of the scattered light intensity was measured at a scattering angle of 173 relative to the laser source. The hydrodynamic radius (*R*) of the particles was estimated from their diffusion coefficient (*D*) using the Stokes−Einstein equation, $D = k_BT/6\pi\eta R$, where k_B is the Boltzmann's constant, *T* is the absolute temperature, and η is the viscosity of the solvent.

Electron Microscopy. A 2 mM solution of **4a** was prepared by dissolution of the compound in double distilled and filtered (0.22 μm) water then sonicated for 15 min. The solution was allowed to stand for 30 min and 2 h. Solutions of **4a** were applied on 200 mesh copper grids coated with resin and a thin carbon layer. A drop of the colloid solution was placed on the grid and allowed to stand for 2 min and then blotted away. Another drop of 10% w/w phosphotungstic acid solution was also placed on the grid and allowed to stand again for 2 min and then blotted away. The specimens were examined using a digital transmission electron microscope. Electron micrographs were taken at a magnification of 60 000−100 000.

EPR Measurements. EPR measurements were carried out on an EPR spectrometer equipped with high sensitivity resonator at room temperature. Unless otherwise indicated, the instrument settings used for general spectral acquisition include the following: microwave power, 10 mW; modulation amplitude, 1 G; receiver gain, 2.0×10^4; scan time, 5.1 s; time constant, 2.6 s; sweep width, 100 G; incremental sweep at 100−300 scans. Spectra were integrated using the WINEPR v.2.11b software. All the spin trapping studies were carried out in DMSO or phosphate buffer (PBS) (10 mM) at pH 7.0 containing 100 μM diethylene triamine pentaacetic acid (DTPA). Sample cells used were 50 μL glass capillary tubes. The spectrum simulation was carried out by an automatic fitting program.[56]

Spin Trapping. (a) Superoxide Radical Anion. (i) Xanthine−Xanthine Oxidase (X−XO). A 50 μL PBS solution contains 100 μM DTPA, 0.4 mM xanthine, 0.5 unit/mL xanthine oxidase, and 20 mM **1. (ii) KO_2 Generating System.** To 20 μL DMSO were added 20 μL of 50 mM stock solution of **4a** or **4b** in DMSO

(56) Rockenbauer, A.; Korecz, L. *Appl. Magn. Reson.* **1996**, *10*, 29–43.

and 10 μL of saturated solution of KO_2 in DMSO. **(b) Hydroxyl Radical.** A 50 μL PBS solution contains 0.3% H_2O_2, 20 mM **4a** or **4b**, and 0.01% $FeCl_2$ solution.

Stopped-Flow Kinetics. Stop-flow technique was used to obtain the apparent spin trapping rate constants of spin traps with superoxide radicals as previously described.[51] KO_2 was used as an $O_2^{\bullet-}$ source and phenol red as a competitor. The growth of the transient absorption at 575 nm from the reaction between $O_2^{\bullet-}$ and phenol red was monitored using UV−vis spectroscopy. The plot was linear during the first 7−9 s. The data were fitted to a linear equation ($t = vx + c$), where v is initial rate of product formation in the presence of various concentrations of spin traps. The resulting initial rates were applied to the following equation $V/v - 1 = (k_{ST}[ST])/(k_{PR}[PR])$, where V is the initial rate of formation in the absence of spin traps; k_{ST} and k_{PR} are rate constants of $O_2^{\bullet-}$ reaction with spin trap and phenol red, respectively, while [ST] and [PR] are the concentrations of spin trap and phenol red (500 uM), respectively.

Decay Kinetics of Various $O_2^{\bullet-}$ Spin Adducts in DMSO. In a typical experiment, 5 μL aqueous solution of a spin trap (20 mM) was added to 45 μL of KO_2 solution in DMSO, which was prepared by mixing 5 μL saturated solution of KO_2 and 40 μL of DMSO. In the case of **4a**, 5 μL of 20 mM **4a** in DMSO solution was used and was added to 45 μL of KO_2 solution (vide supra). To all of the resulting solutions was added 5 μL of water to quench the remaining KO_2. EPR spectra were recorded, and the decay of the $O_2^{\bullet-}$ adduct was then followed by monitoring the decrease of the lowest field peak of the $O_2^{\bullet-}$ adduct. The half-lives were calculated from the first-order rate constants obtained between the fifth and sixth minute of decay.

Computational Studies. All calculations were performed at the Ohio Supercomputer Center. The minimization of initial structures using MMFF94[57] coupled with generalized born/surface area (GB/SA) continuum solvation model using water as the solvent[58] was performed with MacroModel 9.6.[59] The MMFF94 minimized structures were further optimized using Hartree−Fock (HF) self-consistent field method[60] at the HF/3-21G* level of theory using Gaussian 03.[61] The Cartesian coordinates were generated using the GaussView 3.0 Program.

Acknowledgment. This publication was made possible by grant number HL 81248 from the NIH National Heart, Lung, and Blood Institute. This work was supported in part by an allocation of computing time from the Ohio Supercomputer Center.

Supporting Information Available: ^1H, ^{13}C, HSQC, TOCSY, HSQC−TOCSY, HMBC, and ROESY NMR, infrared, high-resolution mass, MS/MS, circular dichroism, and miscellaneous EPR spectra for the compounds as well as Cartesian coordinates for optimized geometries and complete references for 3, 23, 33, and 61. This material is available free of charge via the Internet at http://pubs.acs.org.

(57) Halgren, T. A. *J. Comput. Chem.* **1996**, *17*, 490–519.
(58) Still, W. C.; Tempczyk, A.; Hawley, R. C.; Hendrickson, T. *J. Am. Chem. Soc.* **1990**, *112*, 6127–6129.
(59) *MacroModel 9.6*; Schrödinger, LLC: New York, 2005.
(60) Pople, J. A.; Nesbet, R. K. *J. Chem. Phys.* **1954**, *22*, 571–572.
(61) Frisch, M. J. et al. *Gaussian 03*, revision B.04 ed.; Gaussian, Inc.: Pittsburgh, PA, 2003.